metals

MDPI

Article

The Effects of Three Antibacterial Nanoparticle Coatings on the Surface Characteristics of Stainless Steel

Ahmed Muhsin Yousif Al-Mayali [1,2,*], Ammar S. Kadhum [1] and Thair L. Alzubaydi [3]

[1] Department of Orthodontics, College of Dentistry, University of Baghdad, Baghdad 10047, Iraq; ammar.ortho@codental.uobaghdad.edu.iq
[2] Department of Pediatric, Orthodontics & Prevention Dentistry, College of Dentistry, University of Kufa, Najaf 54001, Iraq
[3] Department of Prosthodontic Dental Technology, Al-Esraa University College, Baghdad 10069, Iraq
* Correspondence: ahmedm.almayali@uokufa.edu.iq

Abstract: The aim of this study is to investigate the antibacterial capabilities of different coating durations of three nanoparticle (NP) coatings: molybdenum (Mo), tantalum (Ta), and zinc oxide (ZnO), and their effects on the surface characteristics of 316L stainless steel (SS). The coated substrates underwent characterization utilizing field emission scanning electron microscopy (FE-SEM), energy dispersive X-ray spectrometry (EDX), and X-ray diffractometer (XRD) techniques. The antibacterial efficacy of NPs was evaluated using the agar diffusion method. The FE-SEM and EDX images confirmed the presence of nano-sized particles of Mo, Ta, and ZnO on the surface of the substrates with perfectly symmetrical spheres and a uniform distribution of the NPs. All groups demonstrated antibacterial activity, and the ability to inhibit the growth of *Streptococcus mutans* and *Lactobacillus acidophilus* bacteria. The ZnO group had the most potent antibacterial effect, followed by the Mo group, while the Ta group had the least effect. A direct-current (DC) plasma sputtering system was used to produce nano-coatings of high purity that were homogeneous, crack-free and showed no sign of delamination. Bacterial strains exposed to Mo, Ta, and ZnO coated surfaces exhibited a significant loss of viability in a time-dependent manner. The optimum sputtering time to ensure the best antibacterial properties and preserve the resources was 1 hour (h) for Mo, 3 h for Ta and 6 h for ZnO.

Keywords: coating; nanomaterial; archwire; molybdenum; tantalum; zinc oxide

check for updates

Citation: Al-Mayali, A.M.Y.; Kadhum, A.S.; Alzubaydi, T.L. The Effects of Three Antibacterial Nanoparticle Coatings on the Surface Characteristics of Stainless Steel. *Metals* **2024**, *14*, 853. https://doi.org/10.3390/met14080853

Academic Editor: Guosong Wu

Received: 23 May 2024
Revised: 7 July 2024
Accepted: 15 July 2024
Published: 25 July 2024

Copyright: © 2024 by the authors. Licensee MDPI, Basel, Switzerland. This article is an open access article distributed under the terms and conditions of the Creative Commons Attribution (CC BY) license (https://creativecommons.org/licenses/by/4.0/).

1. Introduction

It has been postulated that fixed orthodontic appliances might serve as a potential site for plaque accumulation [1]. *S. mutans* and *L. acidophilus* are the main pathogens responsible for dental caries, resulting in a decrease in oral pH levels. The confluence of these factors, forceful contact, irregular tooth enamel surface, and insufficient oral hygiene during orthodontic treatment leads to the demineralization of tooth enamel [2].

In an attempt to control dental biofilm, fluoridated mouth rinse is often prescribed; however, the available mouth rinses may have a high concentration of fluoride, which has the potential to corrode orthodontic devices [3]. Alternatively, nanoparticles (NPs) have been used in the dental field to coat orthodontic archwires, and they have the potential to decrease the number of microbes and thus ultimately reduce the occurrence of caries and periodontal problems in individuals receiving orthodontic treatment [4].

Antibacterial NPs provide effective strategies to address the challenges encountered by conventional antibacterial drugs, such as antibiotic resistance [5]. The unique physio-chemical features of NPs, along with their ability to kill microorganisms, have resulted in a significant increase in research on NPs as possible antibacterial agents [6]. The nanoscale antimicrobials are effectively utilized to manage dental infections due to their bactericidal impact, antiadhesive properties, and prospective capabilities [7].

There are two primary methods for integrating antibacterial NPs into dentistry. One is to directly combine them with materials such as composites, glass ionomers, and topically applied agents. The other is to use them as coatings on surfaces [8,9].

The antibacterial NPs possess a substantial surface area and a high charge density, allowing them to effectively interact with negatively charged bacterial cells. This interaction greatly enhances their antibacterial activity [10]. In addition, the inclusion of antibacterial NPs in polymers or their application as a coating on biomaterial surfaces has been shown to possess exceptional antibacterial properties in the oral cavity [11].

The antibacterial properties of Mo NPs have been documented in previous studies [12,13]. Mo possesses the capacity to impede the growth of several harmful microorganisms, rendering it a potent and durable antibacterial agent for inanimate surfaces; therefore, it has been deemed appropriate for hospital settings [14]. Huang et al. found that Ta alloys exhibit remarkable biocompatibility, making them very efficient as protective coatings in biomedical applications [15]. The utilization of Ta NPs as a protective coating inhibits the growth of Gram-negative bacteria and kills Gram-positive bacteria [16]. Finally, ZnO NPs have demonstrated antibacterial characteristics when used as a coating [17].

Unlike other coating techniques, direct current (DC) plasma sputtering is known to develop a strongly adherent coating on the substrate [18]. The coating thickness is directly proportional to the sputtering duration [19]. Thicker coatings could offer a better antibacterial efficacy, but will consume more resources. To the best of our knowledge, this is the first study to determine the optimum sputtering time to achieve the best antibacterial effect and, at the same time, preserve resources.

This study aimed to investigate the antibacterial and surface characteristics of SS after coating with three different NPs using DC sputtering at three different durations (i.e., coating thicknesses). Moreover, our objective was to identify the coating time that would provide the best antibacterial activity. The current study adopted the null hypothesis that there is no significant difference in antibacterial and surface characteristics between coated and uncoated SS substrates, regardless of the type of NP and sputtering durations used.

2. Materials and Methods

2.1. Study Design

This study involved two steps: first, the surfaces of 316L stainless steel (SS) (316L NO4 ASTM A240 [20], China) substrates were coated and characterized with three different NPs; second, the antibacterial effects of these coatings were tested, and the optimum coating time was identified. The study sample for the test of antibacterial properties consisted of a total of 252 samples, including 216 samples coated with NPs and 36 as control samples (uncoated), as shown in Figure 1. This study included a total of 40 groups, with 20 groups allocated for each test category (biofilm inhibition and inhibition zone); within each test category, 10 groups were designated for each type of bacteria, which were further divided into three subgroups, each representing different NP coatings (Mo, Ta, and ZnO NPs) (Good Fellow Metals Com., London, UK). These subgroups denoted different coating times designated as T1, T2, and T3 for the Mo and Ta groups, and represented 1, 2, and 3 h, respectively. For the ZnO groups, the coating times were 2, 4, and 6 h. Each subgroup included six disks of 316L SS. A control group with three uncoated disks was used for comparison with the respective experimental subgroup.

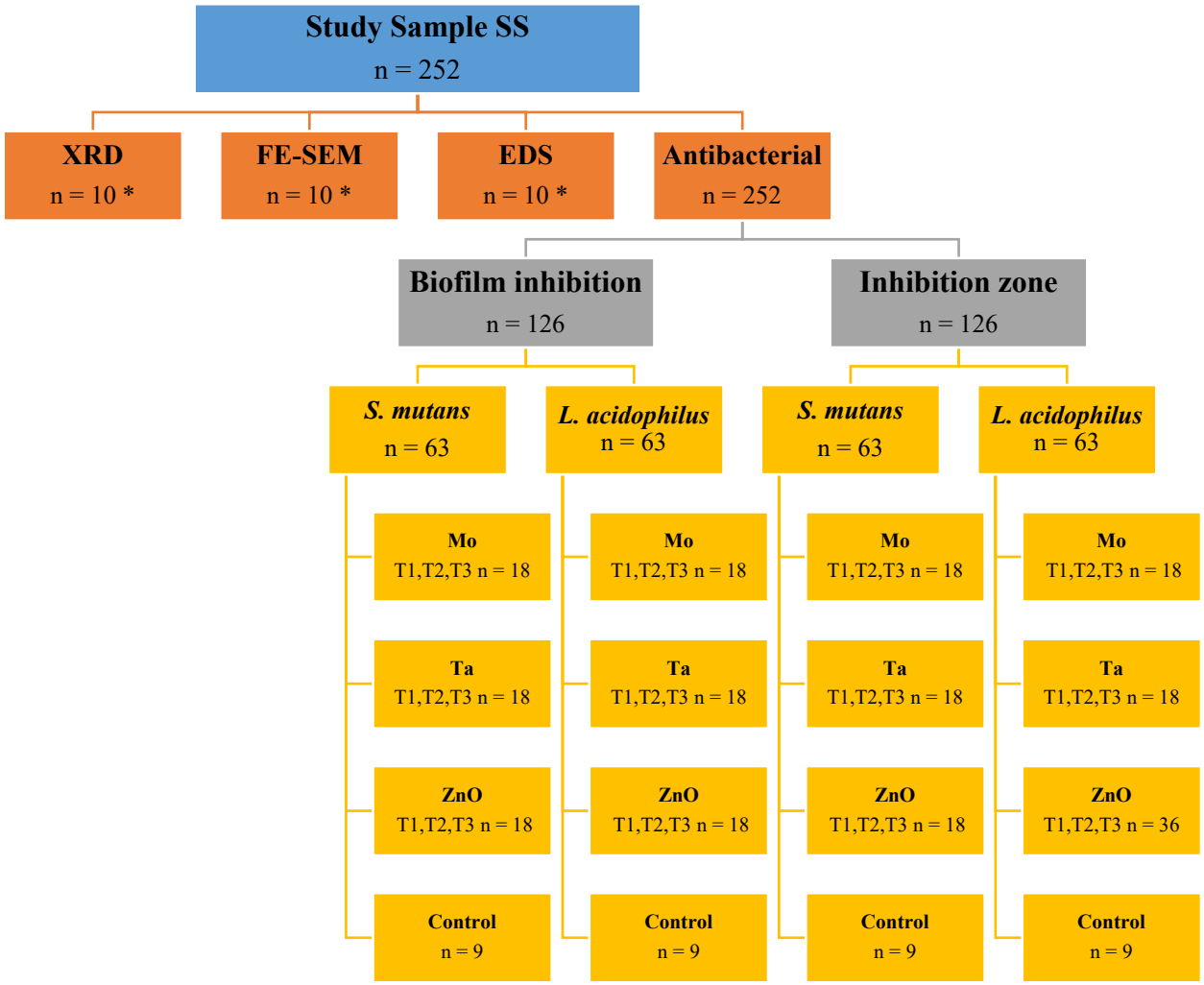


Figure 1. Distribution of the study samples. * The samples used for X-ray diffraction (XRD), field emission scanning electron microscopy (FE-SEM), and energy dispersive X-ray spectrometry (EDX) tests were also used for antibacterial tests.

2.2. Specimen Preparation

This study was carried out on a disk-shaped substrate made of 316L SS. The substrate had a diameter of 10 mm and a thickness of 2 mm. A wire-cutting machine was used to accurately separate and reshape the substrate. To verify that the plate used in this study was made of 316L SS, an analysis of the chemical composition of the 316L SS plate was conducted [21] using spark atomic emission vacuum spectrometry. Mo, Ta, and Zn sheets with high purity (99.9%) were utilized as targets in the sputtering process to produce the NPs. To improve the adhesion between the deposited layer and the surface of the 316L SS material, the substrate samples were sequentially polished using different SiC emery sheets with grit sizes of 120, 400, 600, 800, and 1200 µm [22]. The polishing process was carried out to provide a smooth and highly reflective surface. Immediately before the application of the coating, the samples underwent a cleaning operation to remove any debris and contamination. This was achieved using ultrasonic cleaning (25 kHz, 100% sweep; Elma, Fisher Bioblock Scientific, Scotland, UK) equipment with 99.8% ethanol (Scharlau, Gato Perez, Barcelona, Spain). Subsequently, the samples were allowed to dry at room temperature [23].

2.3. Nanocoating Procedure

Surface modification was achieved by utilizing altered reactive plasma. The sputtering method utilizes a DC reactive plasma device (custom made) to carry out both chemical and physical reactions. Argon gas is classified as an inert gas and was used exclusively as a bombardment agent for the target materials Ta and Mo with the purpose of forming a coating on the substrate material. In addition, argon gas was used in combination with oxygen to make ZnO. A DC power supply with a voltage of 3.5 kilovolts (KV) was utilized to ensure the necessary voltage for the sputtering process.

The polished and immaculate samples were placed in the middle area of the anode electrode's foundation, and the sputtering procedure was started by employing a power supply with a negative voltage of 3.5 kV. After the sputtering technique was complete, the samples were kept in the vacuum chamber until the surrounding temperature was reached. The processed samples were placed in a container to protect them from the surrounding conditions until analysis was performed.

2.4. Characterization of Nanocoated Surfaces

The X-ray diffraction (XRD) investigations were conducted using an X-ray diffractometer (SHIMADZU XRD-6000-Japan, Kyoto, Japan) equipped with a Cu normal focus (NF) X-ray tube with a scanning radius of 185 mm. The X-ray emissions were below 2.5 micro Sieverts per hour at their highest level. The morphological and chemical features of the biomaterials and layers were analyzed using field emission scanning electron microscopy (FE-SEM) (FEI INSPECT F50, Zaragoza, Spain). A software tool for image analysis was utilized to measure the diameters of nanoparticles present on the surface of the coated plate. The elemental distribution of specific spots or sections in the FE-SEM image was analyzed using an energy dispersive X-ray spectrometry (EDX) detector included with the FE-SEM.

2.5. Antibacterial Procedure

The isolated strains underwent analysis utilizing the VITEK 2 compact system (BioMérieux, Inc., Durham, NC, USA). The circular specimens were positioned on top of a freshly cultivated bacterium, specifically *S. mutans* and *L. acidophilus*. Mitis Salivarius Agar (MSA) was employed for *S. mutans*, while deMan Rogosa Sharpe Agar (MRSA) was employed for *L. acidophilus*. After the incubation period, the specimens were taken out of the assay, washed three times by submerging them in Ringer solution, and then placed in a 10 mL tube with 10 mL of PBS. A suspension was created by vortexing the tubes for 15 s. A volume of 100 microliters was spread onto agar plates and then incubated for a period of 48 to 96 h. Subsequently, the inhibitory effectiveness was assessed by detecting microbial cultivation, as described by Morgan et al. [24]. To calculate the microbial cell reduction percentage (R, %), the following equation was used [25]:

$$R\% = \frac{CFU\ control - CFU\ sample}{CFU\ control} \times 100\%$$

* CFU control represents the quantity of viable bacteria present on the uncoated surface.
* CFU sample represents the quantity of viable bacteria present on the coated surface.

For the zone of inhibition test, the specimens were selected from each group according to the parameters established by the CLSI standard [26]. The procedure involved creating solutions of the separated microorganisms with a concentration of 0.5 McFarland standard (1×10^8 bacteria per mL). Four wells, each with a diameter of 10 mm, were made using a sterile cork borer. The specimens with coatings as well as the control were placed in the culture at certain millimeter intervals. Subsequently, the plates were transferred into a candle jar and subjected to incubation at a temperature of 37 °C for 24 h, while maintaining anaerobic conditions. The Vernier caliper was used to measure the diameter of the zone of inhibition surrounding the wells. The test provided an indication of the nanoparticles' antibacterial activities [27].

2.6. Statistical Analyses

The statistical analyses were conducted using SPSS version 26. The Shapiro–Wilk test showed a normal distribution of the data. For inferential statistics, a 95% confidence interval was used with a significance level set to a *p*-value of 0.05, and ANOVA with the Tukey HSD test was used for the comparison of the study groups.

3. Results

3.1. Surface Morphology and Chemical Composition

3.1.1. Characterization Using FE-SEM

The FE-SEM at various magnifications revealed that the coated material was of nanoscale size; the particle size of the NPs varied from 46 to −74 nm for Mo, 16 to −44 nm for Ta, and 16 to −57 nm for ZnO. The NPs took the form of almost perfectly symmetrical spheres with a uniform distribution, as shown in Figure 2.

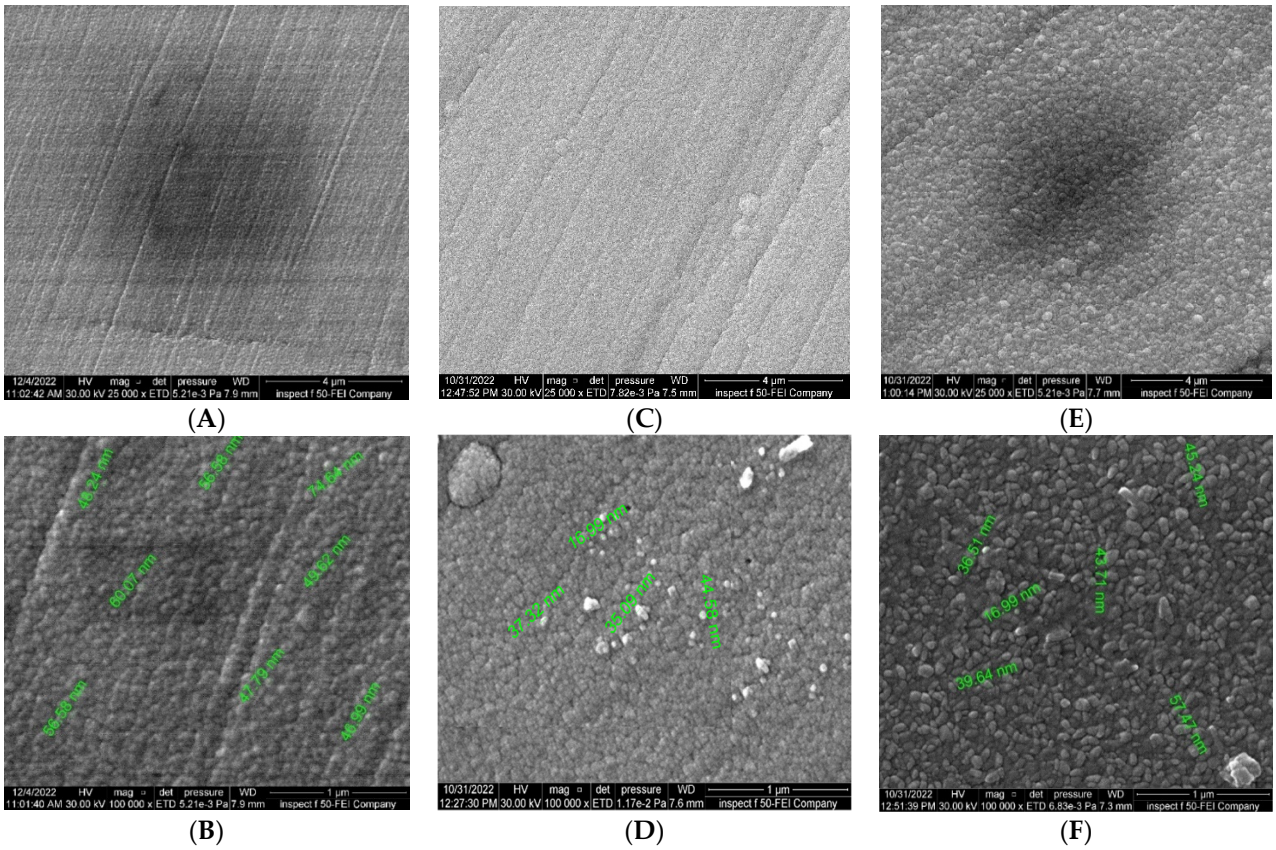


Figure 2. FE-SEM images for the coated stainless steel plate at low- and high-magnification powers: (**A**,**B**) Mo nanoparticles (NPs); (**C**,**D**) Ta NPs; and (**E**,**F**) ZnO NPs.

3.1.2. Characterization via EDX Spectroscopy

The EDX characterization micrographs displayed the chemical elemental analysis and ionic distribution of SS plates coated with Mo, Ta, and ZnO NPs. These findings are shown in Table 1. The deposition of the coating elements was highest in the Ta group, followed by the ZnO group, and lowest in the Mo group. Furthermore, the subgroup with the highest weight percentage (wt%) of the coating material was Ta T3, with a value of 63.0%. Moreover, the subgroup with the lowest wt% was Mo T1, with a value of 6.6%. It should be noted that a reduction was detected in the presence of Fe, which is the main component of the 316L SS alloy.

Table 1. Weight percentages (wt.%) of the elemental composition of molybdenum (Mo), tantalum (Ta), and zinc oxide (ZnO) nanocoatings relative to the amount of Fe on the surface of the 316L SS substrate for various sputtering durations: T1, T2, and T3.

Nanomaterial	Elements (wt.%)	T1	T2	T3
Mo	Mo	6.6	8.0	8.3
	Fe	56.3	53.0	52.7
Ta	Ta	28.5	53.5	63.0
	Fe	37.0	14.2	8.3
ZnO	ZnO	10.6	25.6	30.2
	Fe	50.8	36.8	33.1

T1, T2, and T3 represent 1, 2, and 3 h, respectively, for Mo and Ta, and 2, 4, and 6 h, respectively, for ZnO.

Furthermore, EDX examination revealed the existence of Mo (Figures 3 and 4), Ta (Figures 5 and 6), and ZnO NPs (Figures 7 and 8) on the surfaces of the coated SS samples.

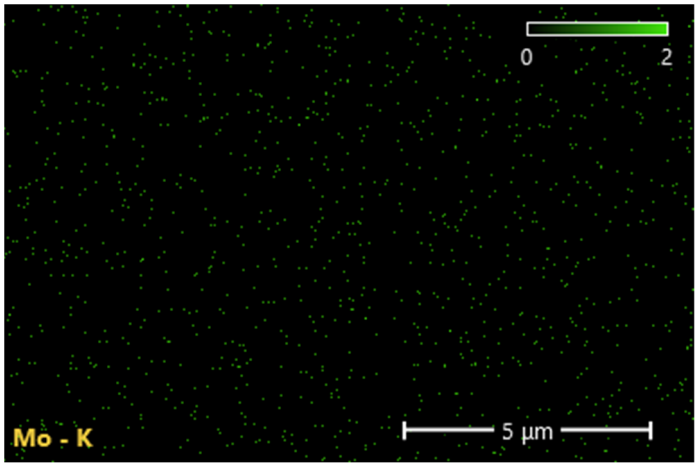


Figure 3. The EDX for the examined SS plate showing the presence of Mo.

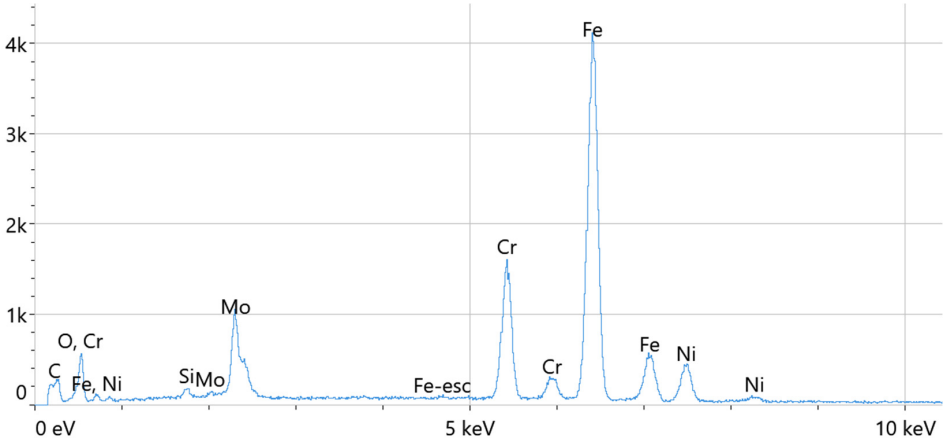


Figure 4. The EDX plot for the examined SS plate coated with Mo.

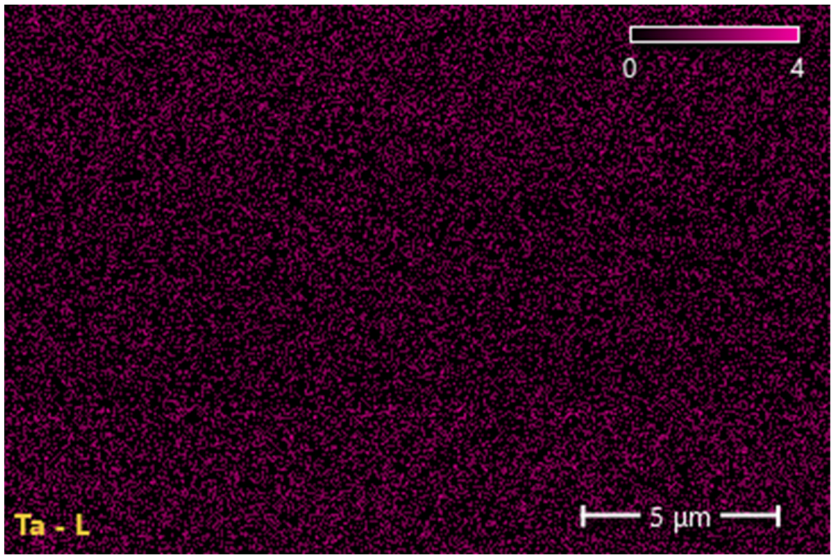


Figure 5. The EDX for the examined SS plate showing the presence of Ta.

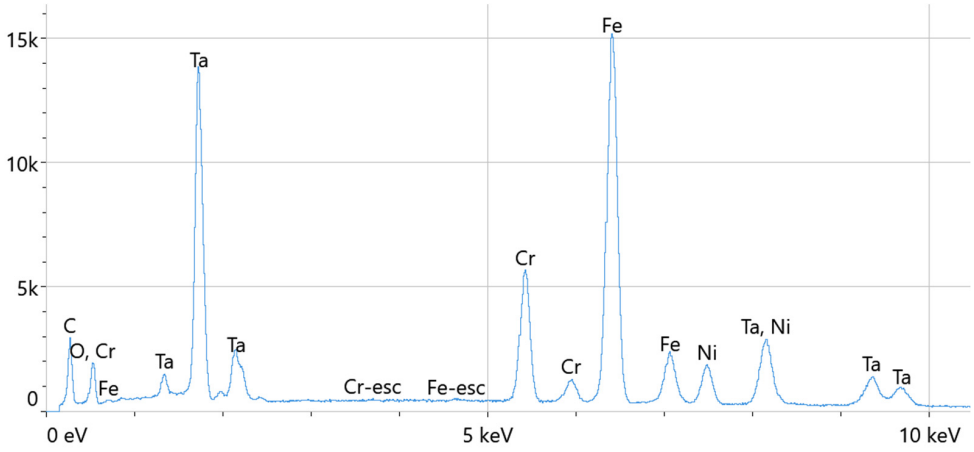


Figure 6. The EDX plot for the examined SS plate coated with Ta.

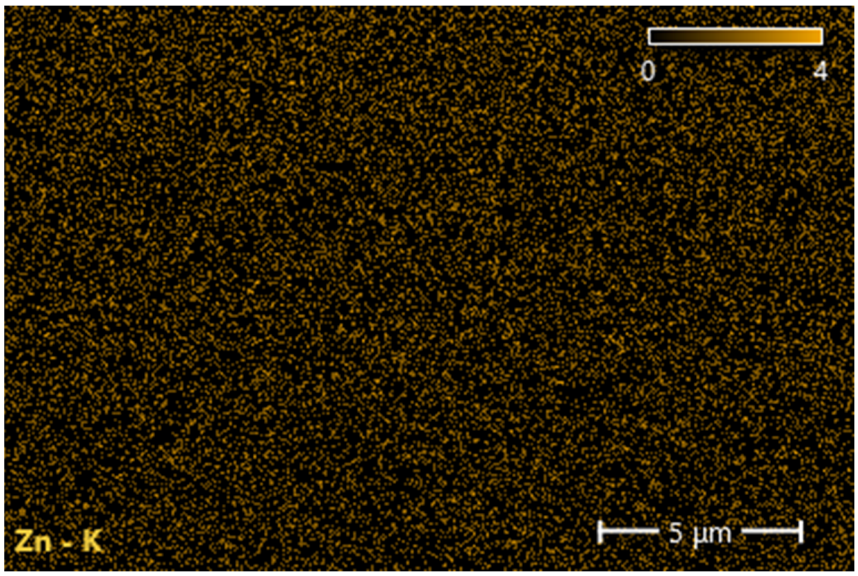


Figure 7. The EDX for the examined SS plate showing the presence of ZnO.

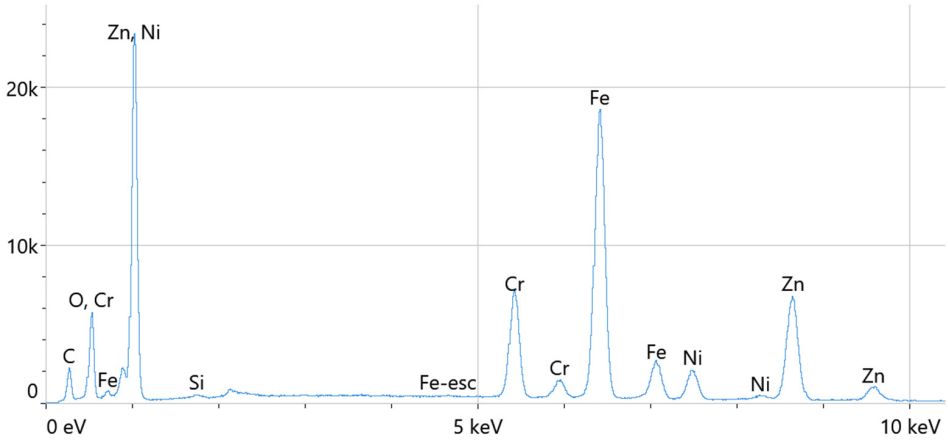


Figure 8. The EDX plot for the examined SS plate coated with ZnO.

3.2. X-ray Diffraction

Figure 9 shows the XRD pattern of 316L SS coated with Ta using plasma sputtering under different sputtering time conditions. It can be observed that the untreated SS exhibits a highly crystalline reflection at 2θ 43.7°, 50.85°, 74.7°, and 90.7°, which can be assigned to (111), (200), (220), and (311) face-centered cubic austenite phases (PDF # ICDD14-0529). Moreover, a (110) body-centered cubic ferrite phase can be observed at 2θ 44.6° (PDF # ICDD 006-0696).

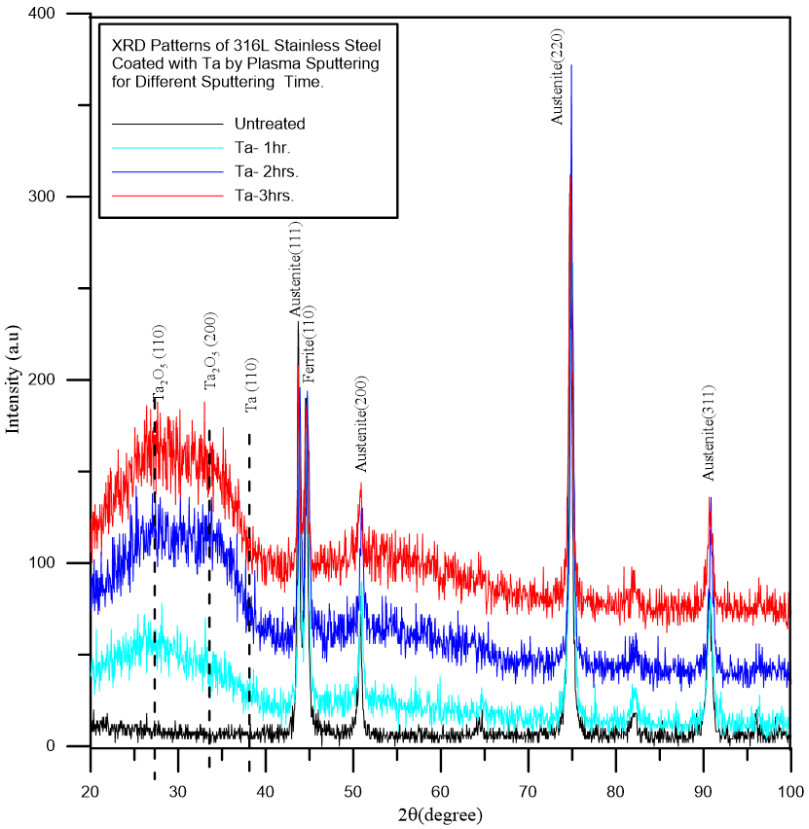


Figure 9. X-ray diffraction pattern of the Ta NPs sputtering coating on the 316L SS substrate at different sputtering times.

The patterns of the Ta-coated specimens (T1, T2, and T3 of sputtering time) clearly show a prominent plateau profile in the range of 2θ 20° to 40°. This profile is a mix of the single-phase Ta (110) at 2θ 38.47°. The deposition of a coating layer of Ta was confirmed

and identified according to the standard Joint Committee on Powder Diffraction Standards (PDF# ICDD 04-0788) and its oxide (110) and (200) Ta_2O_5 (PDF# ICDD 04-0788).

The pattern indicated that the surface of the specimen is well covered with a ZnO layer, and the strongest lines in the pattern of the coated specimen are (100), (002), and (101) at 2θ 31.50, 33.95, and 36.30, respectively (Figure 10). The deposition of a coating layer of ZnO was confirmed and identified (JCPDS-ICDD files # 36-1451). The XRD pattern shows the domination of ZnO in the coated layer, and this is very clear from the (100), (002), and (101) planes.

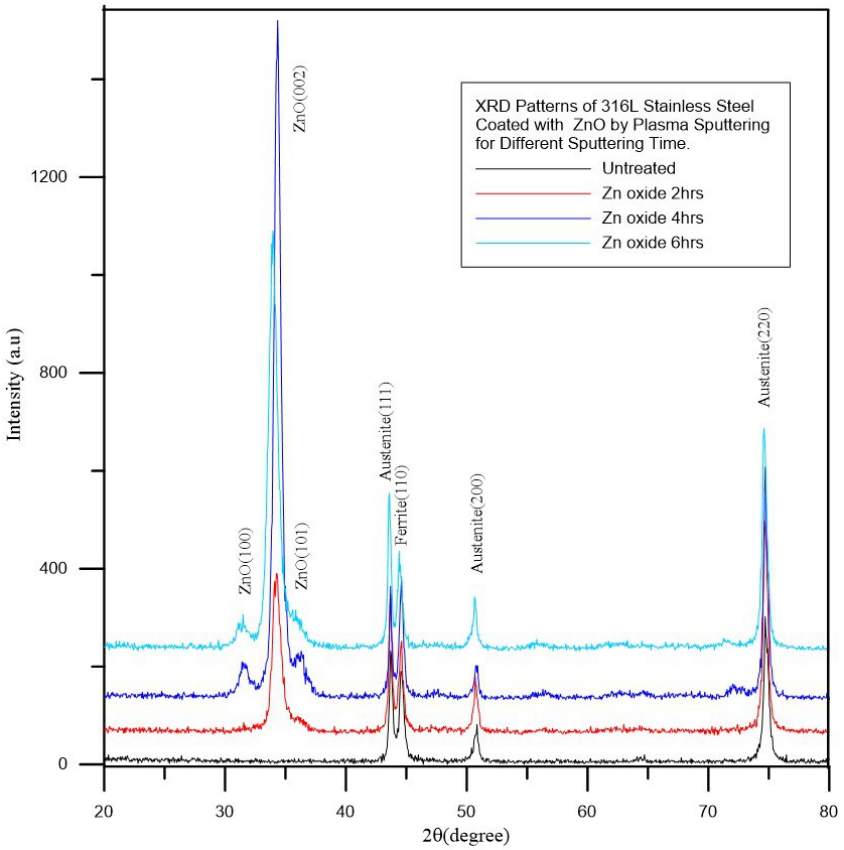


Figure 10. X-ray diffraction pattern of ZnO NPs sputtering coating on the 316L SS substrate at different sputtering times.

Figure 11 shows the XRD pattern of 316L stainless steel Mo coated using plasma sputtering under different sputtering time conditions. A shift in the position of the reflections (Figure 12) of the substrate toward the high 2θ can be observed as the sputtering time increases, forming a Molybdenum oxide (013, 1002, and 202 Mo_4O_{11}) (PDF # ICDD13-0142). The peak shifts identified using XRD diffraction in Figure 12 are located toward the right side of the figure, revealing the lattice strain. The shift is also related to the crystalline size via contraction due to the changes in lattice parameters, which also show an increase in FWHM (Scherrer's formula), corresponding to the higher crystallinity caused by the reduced width and the crystallization process.

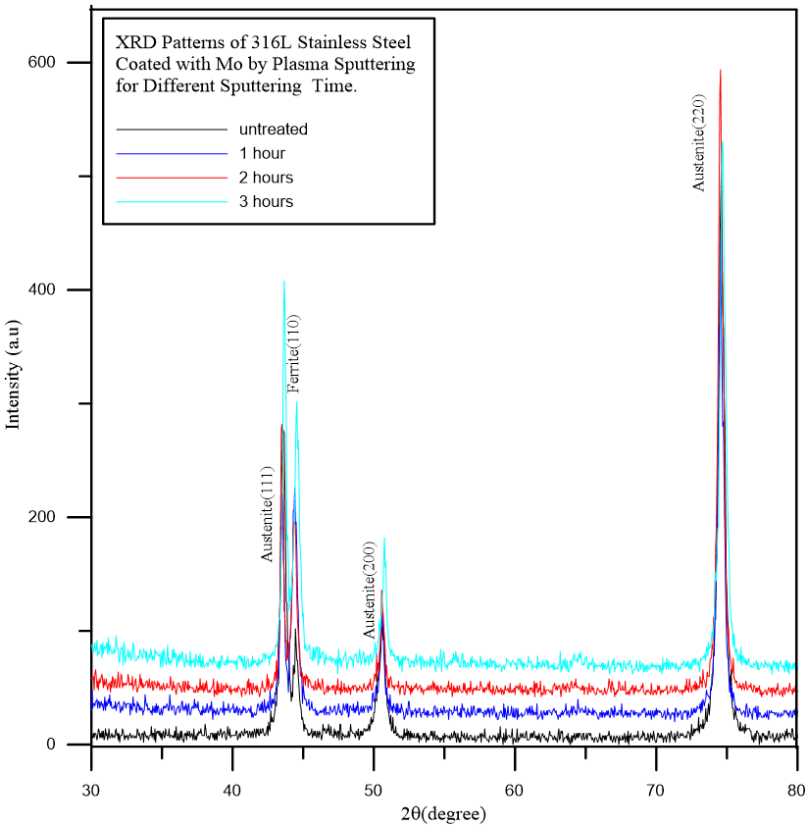


Figure 11. XRD pattern of 316L stainless steel Mo coated using plasma sputtering under different sputtering time conditions.

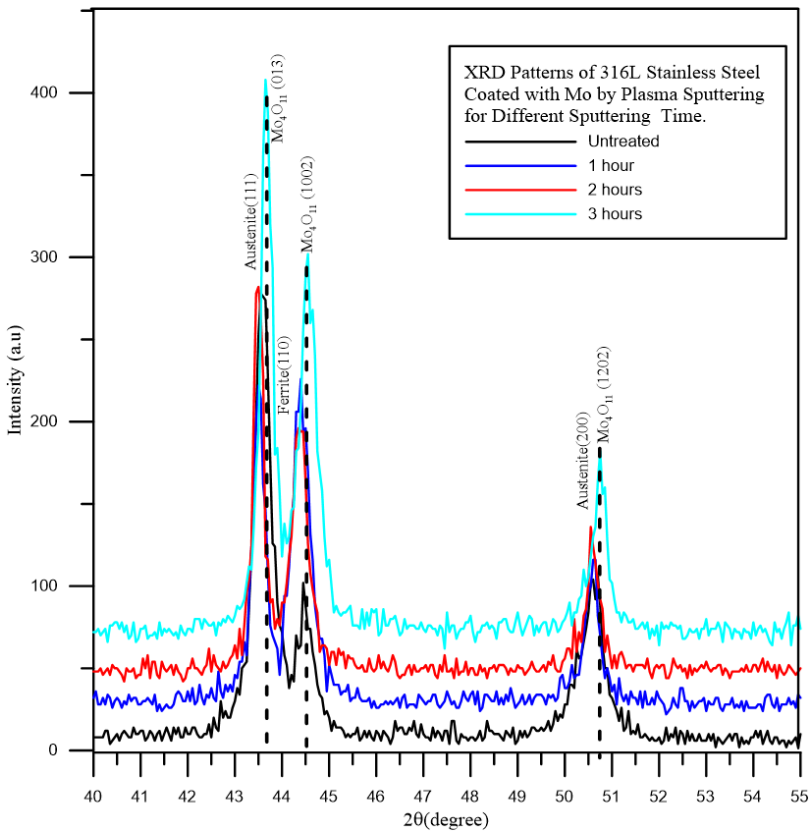


Figure 12. Shift in the peak position of the Mo XRD pattern.

3.3. Microbiological Tests

3.3.1. Antimicrobial Effect of the NP Coating

The Mo, Ta, and ZnO groups have antibacterial activity, including the ability to inhibit the growth of *S. mutans* and *L. acidophilus* bacteria (Table 2). In general, all the tested material demonstrated a stronger antibacterial effect against *S. mutans* rather than *L. acidophilus*. The ZnO group had the most powerful antibacterial effect, followed by the Mo group, and the least was seen in the Ta group. The comparison of mean percentage change across time for *S. mutans* and *L. acidophilus* for ZnO was significant ($p < 0.05$). The antibacterial effect increased with increasing coating duration, indicating that T3 had the most powerful effect for ZnO, as well as for Ta. Conversely, there was no significant difference in the antibacterial effect of Mo for the three sputtering durations.

Table 2. The mean biofilm inhibition percentage (%) of Mo, Ta, and ZnO NP coatings.

Type	Bacteria	Time			ANOVA (p Value)	Tukey HSD		
		T1	T2	T3		T1, T2	T1, T3	T2, T3
Mo	*Streptococcus mutans*	24.6 ± 3.9	24.3 ± 4.4	24.7 ± 8.1	0.99	0.99	0.99	0.99
	Lactobacillus acidophilus	13.2 ± 5.04	13.4 ± 4.6	14.2 ± 4.8	0.9	0.9	0.9	0.9
Ta	*Streptococcus mutans*	8.2 ± 6.12	10.6 ± 5.6	19.8 ± 5.2	0.8	0.8	0.008	0.03
	Lactobacillus acidophilus	2.7 ± 7.6	10.3 ± 4.7	15.7 ± 5.3	0.09	0.09	0.005	0.3
ZnO	*Streptococcus mutans*	27.4 ± 7.1	46.4 ± 5.2	72.1 ± 10.8	0.0001	0.0003	0.00001	0.00003
	Lactobacillus acidophilus	25.95 ± 6.9	39.4 ± 8.5	67.9 ± 6.6	0.0001	0.05	0.0001	0.0001

T1, T2 and T3 represent 1, 2, and 3 h for Mo and Ta. T1, T2 and T3 represent 2, 4, and 6 h for ZnO.

3.3.2. Zone of Inhibition Test

The Mo, Ta, and ZnO groups showed an evident zone of inhibition effect when compared with the control group (Figure 13). In general, all the tested materials showed a stronger inhibition zone effect against *S. mutans* compared to *L. acidophilus*. However, the ZnO group had the strongest inhibition zone effect, followed by the Ta and Mo groups which showed similar effects.

The comparison of the inhibition zone for *S. mutans* with Mo showed no significant difference, while for *L. acidophilus* it was significantly lower in T1 than in T2 and T3 (Figure 14). The comparison of the inhibition zone for *S. mutans* with Ta was significantly lower in T1 than in T2 and T3, while for *L. acidophilus* it was significantly lower in T1 compared to T3 only (Figure 15). The comparison of the inhibition zone with ZnO according to the type of bacteria was significant for T1, T2 and T3 ($p < 0.05$). The comparison of the inhibition zone for *S. mutans* and *L. acidophilus* with ZnO was significantly higher for T3 than for T1 and T2. The inhibition zone was shown to increase with increasing sputtering time (Figure 16).

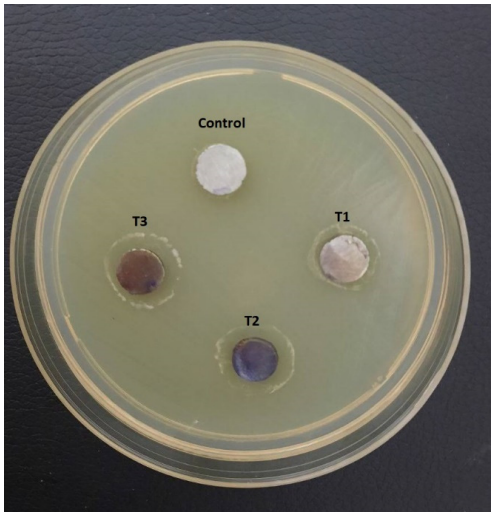


Figure 13. The inhibition zones of three different timing of Zinc oxide nanoparticles coatings against *S. mutans*: T1 (2 h): 1.4 cm, T2 (4 h): 1.6 cm, and T3 (6 h): 1.8 cm.

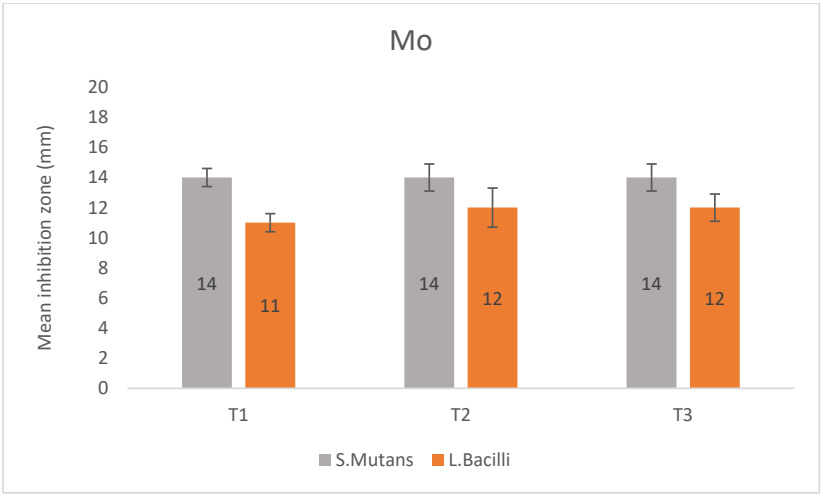


Figure 14. The mean inhibition zones in the antibacterial test for Mo nanoparticles. T1, T2, and T3 represent 1, 2, and 3 hours of coating time.

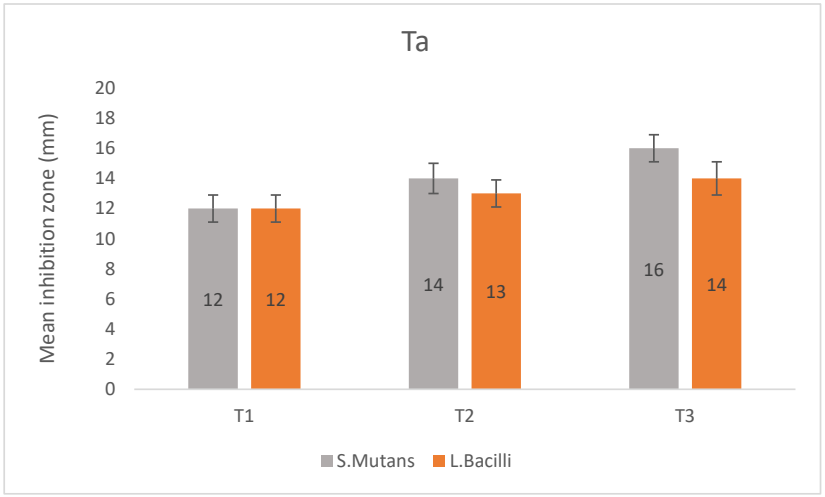


Figure 15. The mean inhibition zones in the antibacterial test for Ta nanoparticles. T1, T2, and T3 represent 1, 2, and 3 hours of coating time.

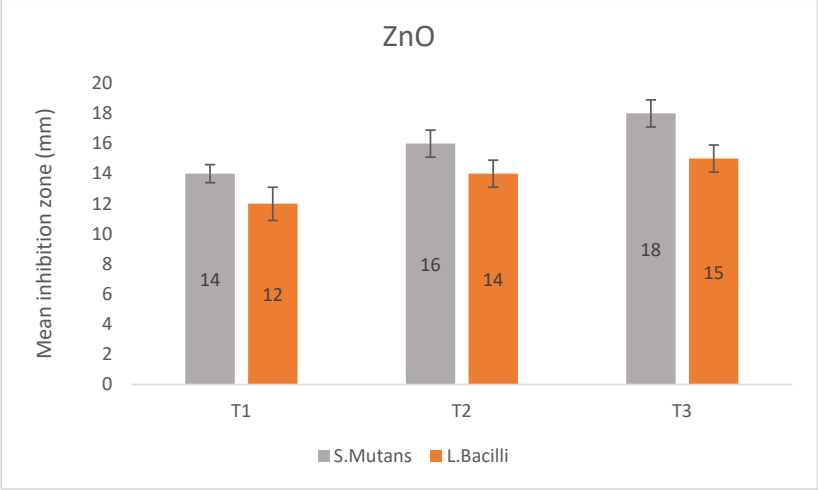


Figure 16. The mean inhibition zones in the antibacterial test for ZnO nanoparticles. T1, T2 and T3 represent 2, 4, and 6 hours of coating time.

4. Discussion

The current study demonstrated the significant effect of different nanomaterials on antibacterial properties, and this effect mostly increases with a longer DC sputtering time (i.e., coating thickness). The *S. mutans* bacterium chosen for this investigation is considered a cariogenic pathogen that plays a primary role in the formation of human dental caries, primarily due to its robust ability to produce biofilms [28]. *L. acidophilus* has been found to be the second most cariogenic bacterium in the oral cavity flora and plays a major role in the advanced stages of caries. After the initiation of demineralization, there is an elevation of *L. acidophilus* bacteria and a reduction in *S. mutans* bacteria [29].

Due to progress in nanotechnology, nanocoatings have emerged as a possible remedy for addressing therapeutic challenges [30]. Therefore, the use of surface coating technology is highly important in clinical applications [31]. Magnetron sputtering is a widely employed process for depositing thin films onto SS surfaces, enabling the coating of surfaces with various geometries. Magnetron-sputtered films frequently outperform films formed using alternative physical vapor deposition (PVD) technologies and can offer functionality comparable to that of much thicker films produced using different surface coating procedures. Furthermore, a diverse selection of metals and metal alloys can serve as a source material to generate NPs to produce thin micrometer (μm) coating layers suitable for a variety of applications [32,33]. The properties of the coating can be modified by altering the duration of the sputtering or the prevailing circumstances [33,34].

The selection of Mo, Ta, and ZnO NPs depends on their potential to form a robust layer and enhance the sustained release of NPs [14,16,35,36]. Several publications have documented that Mo has antibacterial properties [12,13], and can inhibit the growth of many perilous microorganisms, making it a potent and durable antibacterial agent for inanimate surfaces [14]. Moreover, Ta coatings have exhibited excellent antibacterial properties [37]; Ta alloys have remarkable biocompatibility [15] and the ability to suppress the proliferation of Gram-negative bacteria and kill Gram-positive bacteria [16]. ZnO is attractive due to its good biocompatibility, minimal toxicity, and antimicrobial properties [36].

To improve the bond between the coated layer and the surface of the 316L SS material, all the discs were successively abraded and finished to a mirror-polished surface [22]. Ultrasonication in deionized water was performed to remove any contaminants [23]. UV light was used to sterilize the SS plates due to its efficacy; moreover, since UV light involves no heat or chemicals, this method ensures that the samples maintain their properties [38].

The FE-SEM images confirmed the presence of NPs for all the tested materials, namely, Mo, Ta, and ZnO. Furthermore, the FE-SEM and EDX analyses confirmed the high purity of the coating, as well as its uniformity, compactness, and homogeneity. The existence

of surface voids or gaps in the coating is a common cause of material failures [39]; these were not detected in any of the tested groups. Therefore, it can be assumed that the DC sputtering method made it possible to effectively obtain a tight and uniform coating.

The elemental analysis of the experimental groups, as compared to the control groups, detected the presence of Mo, Ta, and ZnO atoms on the coated SS plates, with the highest wt.% observed for Ta and the lowest ionic distribution concentration for Mo. The wt.% of the Mo, Ta, and ZnO increased as the duration of sputtering progressed, with a decrease in the amount of Fe (which makes up the majority of the 316L SS alloy); this result is in agreement with the findings of Cao and Zhou [40]. The variation in the wt.%. can be explained by the variable surface binding energy (SBE) of the different metals used. The SBE refers to the minimum energy needed to separate a particle from a group of particles or to break down a group of particles into their individual components [41]. Therefore, the largest amount of coating was deposited using Ta, which has the lowest SBE (21.8 eV) among the targets used [42].

The 316L SS substrate was characterized using an X-ray diffraction profile. The XRD verified the lack of any phase transformation throughout the coating process. Furthermore, the analysis revealed the absence of peaks associated with impurities in the X-ray diffraction pattern, which verified the successful production of very pure Mo, Ta, and ZnO utilizing the sputtering coating technique. Sputtering is a versatile and widely used thin film deposition technique with several advantages, including high purity, precise control, and uniformity [43]; moreover, this technique can produce thin films and super-lattices of complex oxides, and usually at a lower cost than other methods [44].

The Molybdenum oxide formation may be due to the presence of oxygen traces in the sputtering process and the tendency of Mo metal to oxidize in the atmosphere before the diffraction analysis is complete. This shift can be attributed to different reasons. First, the lattice parameter of the crystals causes a slight displacement in the peaks through doping (introduction of Mo atoms into the Fe crystal), changes in stoichiometry, and the composition of the surface. The shifts in the peaks are influenced by defects, stress, and composition, which in turn are affected by changes in lattice parameters. The diffraction shifts to the right or left are caused by the difference in ionic radii between the original elements (Fe) and the dopant ions (Mo). This shift can lead to an increase or decrease in the size of the crystal. The shifts can be attributed to the substitution of elements or the presence of non-stoichiometric phases and structural transformations. Additionally, the shifts to the left or right of the 2θ angles can result in changes in the full width at half maximum (FWHM), and the peak height has a direct impact on the qualities of the crystals, either by enhancing or diminishing them.

The crystallite size is inversely proportional to the FWHM; therefore, the smaller the FWHM (which means the sharper the peak), the greater the crystallite dimensions. Third, the shift towards the right (with a higher 2θ value) resulted in a contraction of the concentration and enhanced the crystal characteristics (characterization) due to alterations in the lattice parameters [45].

Recently, many methods have been devised to combat antimicrobial resistance. One of these methods involves exploring the potential of nanomaterials as alternative antibacterial agents. In vitro studies have shown that nanomaterials have harmful effects on several types of bacteria, indicating their potential use in medical applications such as delivering drugs and the creation of artificial tissues or organs [46–48].

The current study demonstrates that the application of Mo, Ta, and ZnO NP coatings exhibits significant antibacterial effects against Gram-positive bacteria *S. mutans* and *L. acidophilus*. The NPs have excellent characteristics and can improve interactions with cells and optimize antibacterial activity due to increased contact surface area [49]. Studies on the antibacterial effects of Mo NPs are significantly less extensive compared to other inorganic substance NPs. One study found the antibacterial activity of Mo NPs to be active against *P. mirabilis* and *K. pneumonia*, showing a clear zone of inhibition [50]. Moreover, MoO_3 paint exhibited good antibacterial properties against pathogenic bacteria including *E. coli*,

S. aureus, and *K. pneumonia* [35]. An antibacterial study suggested that the effectiveness of Mo is due to the presence of hydroxonium ions, which is caused by the production of Mo on the surface [12].

This study demonstrates the antibacterial activity of Ta NPs, and the results are in agreement with a study showing that amorphous tantalum oxide coatings exhibited excellent antibacterial properties [51,52]. The reactive oxygen species (ROS) may be the key factor of Ta NPs regulation in the microenvironment. These findings indicate that Ta NPs have the potential to be used in tissue engineering and inflammation therapy [53].

It is crucial to emphasize that the antimicrobial impact of the ZnO NP coating on *S. mutans* and *L. acidophilus* was notably greater compared with the coating of Ta and Mo NPs, and was more potent in suppressing the formation of biofilms in the T3 coating time group. Kasraei et al. found that the inclusion of ZnO NP in the dental compound had a substantial antibacterial effect on *S. mutans* [54]. The antibacterial action of ZnO NPs is attributed to the physical disruption of the cell membrane and the generation of ROS within the cell. ZnO NPs often have an isoelectric point above nine and display significant positive surface charges in physiological settings. This facilitates electrostatic interactions with the negatively charged surface of bacteria [55,56].

In this study, the efficiency of biofilm suppression was assessed by comparing the different time durations of the Mo, Ta, and ZnO NP coatings with a control standard. Furthermore, we observed that, with an increase in sputtering time, the bacterial viability exhibited a significant drop and the biofilm inhibition size increased similarly for the Ta and ZnO groups; with the best antibacterial effect being for the T3 duration for both of them, this clearly illustrates the time-dependency of the antibacterial activity. However, the increase in the duration of sputtering had a limited impact on the suppression of the Mo group biofilm; this effect may be due to the higher SBE of Mo, limiting the thickness of the coating, hence resulting in limited biofilm inhibition.

In summary, based on the findings of this study, the ideal sputtering coating times are T1 for Mo, and T3 for Ta and ZnO.

5. Conclusions

(1) The DC plasma sputtering system can be used to produce high purity, homogeneous, crack-free nano-coatings of Mo, Ta, and ZnO on 316L SS, with no sign of delamination.
(2) The amount of nanocoating deposited on the substrate is dependent on two factors: coating duration and the type of NP used.
(3) Bacterial strains exposed to surfaces that have been coated with Mo, Ta, and ZnO show a noticeable decrease in their ability to sustain life in a time-dependent manner.
(4) The antibacterial impact of the ZnO NP coating on *S. mutans* and *L. acidophilus* is notably greater than that of Ta and Mo NP coatings.
(5) The optimum sputtering coating times to ensure the best antibacterial effect and preserve resources are T1(1) hour for Mo, T3 for Ta (3 h), and T3 (6 h) for ZnO.

Author Contributions: Conceptualization: A.M.Y.A.-M., A.S.K. and T.L.A.; methodology: A.M.Y.A.-M., A.S.K. and T.L.A.; software: A.M.Y.A.-M. and T.L.A.; validation: A.M.Y.A.-M., A.S.K. and T.L.A.; formal analysis: A.M.Y.A.-M., A.S.K. and T.L.A.; investigation: A.M.Y.A.-M. and T.L.A.; resources: A.M.Y.A.-M. and T.L.A.; data curation: A.M.Y.A.-M., A.S.K. and T.L.A.; writing—original draft preparation: A.M.Y.A.-M.; writing—review and editing: A.S.K.; visualization: A.S.K. and T.L.A.; supervision: A.S.K. and T.L.A. project administration: A.S.K. and T.L.A.; funding acquisition: A.M.Y.A.-M. All authors have read and agreed to the published version of the manuscript.

Funding: This research received no external funding.

Data Availability Statement: The original contributions presented in the study are included in the article, further inquiries can be directed to the corresponding author.

Conflicts of Interest: The authors declare no conflict of interest.

References

1. Ristic, M.; Vlahovic, S.; Sasic, M.; Zelic, O. Clinical and microbiological effects of fixed orthodontic appliances on periodontal tissues in adolescents. *Orthod. Craniofacial Res.* **2007**, *10*, 187–195. [CrossRef] [PubMed]
2. Toi, C.; Mogodiri, R.; Cleaton-Jones, P.E. Mutans streptococci and lactobacilli on healthy and carious teeth in the same mouth of children with and without dental caries. *Microb. Ecol. Health Dis.* **2009**, *12*, 35–41. [CrossRef]
3. Farzin, H.; Mohamad Hadi, M.; Nima, M. Effect of fluoride on nickel-titanium and stainless steel orthodontic archwires: An in-vitro study. *J. Dent.* **2015**, *12*, 49–59.
4. Borzabadi-Farahani, A.; Borzabadi, E.; Lynch, E. Nanoparticles in orthodontics, a review of antimicrobiological and anti-caries application. *Acta Odontol. Scand.* **2014**, *72*, 413–417. [CrossRef] [PubMed]
5. Bapat, R.A.; Joshi, C.P.; Bapat, P.; Chaubal, T.V.; Pandurangappa, R.; Jnanendrappa, N.; Gorain, B.; Khurana, S.; Kesharwani, P. The use of nanoparticles as biomaterials in dentistry. *Drug Discov. Today* **2019**, *24*, 85–98. [CrossRef] [PubMed]
6. Nambi, N.; Shrinivaasan, N.R.; Dhayananth, L.X.; Chajallani, V.G.; George, A.M. Renaissance in orthodontics: Nanotechnology. *Int. J. Orthod. Rehabil.* **2016**, *7*, 139.
7. Bhattacharya, M.; Seong, W.J. Carbon nanotube-based materials—Preparation, biocompatibility, and applications in dentistry. In *Nanobiomaterials in Clinical Dentistry*, 2nd ed.; Elsevier: Amsterdam, The Netherlands, 2019; pp. 41–76.
8. Hannig, M.; Kriener, L.; Hoth-Hannig, W.; Becker-Willinger, C.; Schmidt, H. Influence of nanocomposite surface coating on biofilm formation in situ. *J. Nanosci. Nanotechnol.* **2007**, *7*, 4642–4648. [CrossRef]
9. Monteiro, D.R.; Gorup, L.F.; Takamiya, A.S.; Ruvollo-Filho, A.C.; Camargo, E.R.; Barbosa, D.B. The growing importance of materials that prevent microbial adhesion: Antimicrobial effect of medical devices containing silver. *Int. J. Antimicrob. Agents* **2009**, *34*, 103–110. [CrossRef] [PubMed]
10. Cao, W.; Zhang, Y. Novel resin-based dental material with anti-biofilm activity and improved mechanical property by incorporating hydrophilic cationic copolymer functionalized nanodiamond. *J. Mater. Sci. Mater. Med.* **2018**, *29*, 162. [CrossRef]
11. Saafan, A.; Zaazou, M.H.; Sallam, M.K.; Mosallam, O.; El Danaf, H.A. Assessment of Photodynamic Therapy and Nanoparticles Effects on Caries Models. *Maced. J. Med. Sci.* **2018**, *6*, 1289–1295. [CrossRef]
12. Zollfrank, C.; Gutbrod, K.; Wechsler, P.; Guggenbichler, J.P. Antimicrobial activity of transition metal acid MoO_3 prevents microbial growth on material surfaces. *Mater. Sci. Eng.* **2012**, *C32*, 47. [CrossRef] [PubMed]
13. Qureshi, N.; Patil, R.; Shinde, M. Innovative biofilm inhibition and anti-microbial behavior of molybdenum sulfide nanostructures generated by microwave-assisted solvothermal route. *Appl. Nanosci.* **2015**, *5*, 331. [CrossRef]
14. Shafaei, S.; Lackner, M.; Meier, M.; Plank, J.; Guggenbichler, J.; Zollfrank, C. Polymorphs of molybdenum trioxide as innovative antimicrobial materials. *Surf. Innov.* **2013**, *1*, 202. [CrossRef]
15. Huang, H.; Chang, Y.; Lai, M.; Lin, C.; Lai, C.; Shieh, T. Antibacterial TaN-Ag coatings on titanium dental implants. *Surf. Coat. Technol.* **2010**, *205*, 1636–1641. [CrossRef]
16. Shanaghi, A.; Souri, A.R.; Saedi, H.; Chu, P.K. Effects of the tantalum intermediate layer on the nanomechanical properties and biocompatibility of nanostructured tantalum/tantalum nitride bilayer coating deposited by magnetron sputtering on the nickel titanium alloy. *Appl. Nanosci.* **2021**, *11*, 1867–1880. [CrossRef]
17. Ramazanzadeh, B.; Jahanbin, A.; Yaghoubi, M.; Shahtahmassbi, N.; Ghazvini, K.; Shakeri, M.; Shafaee, H. Comparison of antibacterial effects of ZnO and CuO nanoparticles coated brackets against *Streptococcus mutans*. *J. Dent.* **2015**, *16*, 200.
18. Rossnagel, S. Sputter Deposition. In *Opportunities for Innovation: Advanced Surface Engineering*; Sproul, W.D., Legg, K.O., Eds.; Technomic Publishing Co.: Lancaster, PA, USA, 1995.
19. Geisler, M.; Braatz, C.; Bruch, J.; Kastner, A.; Kress, M.; Ruske, M.; Willms, T.; Zmelty, A. Meeting the demands of modern large area glass coating: Latest developments of horizontal and vertical coaters and applications. *Thin Solid Films* **2003**, *442*, 15–20. [CrossRef]
20. *ASTM A240*; Standard Specification for Chromium and Chromium-Nickel Stainless Steel Plate, Sheet, and Strip for Pressure Vessels and for General Applications. ASTM International: West Conshohocken, PA, USA, 2022.
21. *ASTM E-1086*; Standard Test Method for Analysis of Austenitic Stainless Steel by Spark Atomic Emission Spectrometry. ASTM International: West Conshohocken, PA, USA, 2022.
22. Khan, A.S.; Awais, M. Low-cost deposition of antibacterial ion-substituted hydroxyapatite coatings onto 316L stainless steel for biomedical and dental applications. *Coatings* **2020**, *10*, 880. [CrossRef]
23. Oliveira, D.; Thomson, J.; Alhabeil, J. In vitro Streptococcus mutans adhesion and biofilm formation on different esthetic orthodontic archwires. *Angle Orthod.* **2021**, *91*, 786–793. [CrossRef]
24. Morgan, T.; Wilson, M. The effects of surface roughness and type of denture acrylic on biofilm formation by Streptococcus oralis in a constant depth film fermentor. *J. Appl. Microbiol.* **2001**, *91*, 47–53. [CrossRef]
25. Stanković, A.; Dimitrijević, S.; Uskoković, D. Influence of size scale and morphology on antibacterial properties of ZnO powders hydrothemally synthesized using different surface stabilizing agents. *Colloids Surf. B Biointerfaces* **2013**, *102*, 21–28. [CrossRef] [PubMed]
26. Clinical and Laboratory Standards Institute (CLSI). *Performance Standards for Antimicrobial Susceptibility Testing*; CLSI Supplement M100-ED-34; Clinical and Laboratory Standards Institute: Wayne, PA, USA, 2024.

27. Balouiri, M.; Sadiki, M.; Ibnsouda, S.K. Methods for in vitro evaluating antimicrobial activity: A review. *J. Pharm. Anal.* **2016**, *6*, 71–79. [CrossRef]
28. Aqawi, M.; Sionov, R.; Gallily, R.; Friedman, M.; Steinberg, D. Anti-Bacterial properties of Cannabigerol toward *Streptococcus mutans*. *Front. Microbiol.* **2021**, *12*, 656471. [CrossRef] [PubMed]
29. Ahirwar, S.; Gupta, M.; Snehi, S. Dental caries and *lactobacillus*: Role and ecology in the oral cavity. *Int. J. Pharm. Sci. Res.* **2019**, *10*, 4818–4829.
30. He, L.; Dai, D.; Xie, L.; Chen, Y.; Zhang, C. Biological effects, applications and strategies of nano modification of dental metal surfaces. *Mater. Des.* **2021**, *207*, 109890. [CrossRef]
31. Zhang, R.; Han, B.; Liu, X. Functional Surface Coatings on Orthodontic Appliances: Reviews of Friction Reduction, Antibacterial Properties, and Corrosion Resistance. *Int. J. Mol. Sci.* **2023**, *24*, 6919. [CrossRef] [PubMed]
32. Mattox, D. Ion plating and ion beam-assisted deposition. In *Handbook of Physical Vapor Deposition (PVD) Processing*; William Andrew Publishing Norwich: Norwich, NY, USA, 2010; pp. 301–331.
33. Zeng, S.; Yang, Z.; Hou, Z. Dynamic multifunctional devices enabled by ultrathin metal nanocoatings with optical/photothermal and morphological versatility. *Proc. Natl. Acad. Sci. USA* **2022**, *119*, 4. [CrossRef] [PubMed]
34. Yahya, K. Effect of electrode separation in magnetron DC plasma sputtering on grain size of gold coated samples. *Iraqi J. Phys.* **2018**, *15*, 202–210. [CrossRef]
35. Karthikeyan, K.; Mariappan, P.; Murugan, V.; Sang Jae, K. Nanostructured molybdenum oxide-based antibacterial paint: Effective growth inhibition of various pathogenic bacteria. *Nanotechnology* **2014**, *25*, 15101.
36. Kachoei, M.; Divband, B.; Rahbar, M.; Esmaeilzadeh, M.; Ghanizadeh, M.; Alam, M. A Novel Developed Bioactive Composite Resin Containing Silver/Zinc Oxide (Ag/ZnO) Nanoparticles as an Antimicrobial Material against *Streptococcus mutans*, *Lactobacillus*, and *Candida albicans*. *Evid.-Based Complement. Altern. Med.* **2021**, *2021*, 4743411. [CrossRef]
37. Chang, Y.; Huang, H.; Chen, H.; Lai, C.; Wen, C. Antibacterial properties and cytocompatibility of tantalum oxide coatings. *Surf. Coat. Technol.* **2014**, *259*, 193. [CrossRef]
38. Ardeshna, A.; Chavan, K.; Prakasam, A.; Ardeshna, D.; Shah, D.; Velliyagounder, K. Effectiveness of Different Sterilization Methods on Clinical Orthodontic Materials. *J. Indian Orthod. Soc.* **2023**, *57*, 98–105. [CrossRef]
39. Wadhwa, P.; Sharma, S.; Sahu, S.; Sharma, A.; Kumar, D. A Review of Nanoparticles Characterization Techniques. *Curr. Nanomater.* **2022**, *7*, 202–214. [CrossRef]
40. Cao, Y.; Zhou, C. Thickness dependence of surface roughness and magnetic properties of FeNiCr thin films. *J. Magn. Magn. Mater.* **2013**, *333*, 1–7. [CrossRef]
41. Rohlf, J.W. *Modern Physics from α to Z*; John Wiley & Sons: Hoboken, NJ, USA, 1994; p. 20.
42. Transition Metal Elements. 2022. Available online: https://www.thermofisher.com/iq/en/home/materials-science/learning-center/periodic-table/transition-metal.html (accessed on 20 June 2022).
43. Pujahari, R. *Solar Cell Technology. Energy Materials*; Science Direct; Elsevier: Amsterdam, The Netherlands, 2021.
44. Mukhtiar, S.; Yogita, S.; Hitesh, V.; Maninder, S. Various sputtered coating deposition techniques for the development of boron nitride based thin film coating: A review. *AIP Publ.* **2024**, *2986*, 020008.
45. Vashista, M.; Soumitra, P. Correlation between full width at half maximum (FWHM) of XRD peak with residual stress on ground surfaces. *Philos. Mag.* **2012**, *92*, 4194–4204. [CrossRef]
46. Vimbela, G.; Ngo, S.; Fraze, C.; Yang, L.; Stout, D. Antibacterial Properties and Toxicity from Metallic Nanomaterials. *Int. J. Nanomed.* **2017**, *12*, 3941–3965. [CrossRef] [PubMed]
47. Nocito, G.; Sciuto, E.; Franco, D.; Nastasi, F.; Pulvirenti, L.; Petralia, S.; Spinella, C.; Calabrese, G.; Guglielmino, S.; Conoci, S. Physicochemical Characterization and Antibacterial Properties of Carbon Dots from Two Mediterranean Olive Solid Waste Cultivars. *Nanomaterials* **2022**, *12*, 885. [CrossRef] [PubMed]
48. Agnihotri, S.; Dhiman, N. Development of Nano-Antimicrobial Biomaterials for Biomedical Applications. In *Advances in Biomaterials for Biomedical Applications*; Tripathi, A., Melo, J.S., Eds.; Advanced Structured Materials; Springer: Singapore, 2017; pp. 479–545.
49. Da Silva, B.; Caetano, B.; Chiari-Andréo, B.; Linhari Rodrigues, R.; Chiavacci, L. Increased Antıbacterial Activity of Zno Nanoparticles: Influence of Size and Surface Modification. *Colloids Surf. B Biointerfaces* **2019**, *117*, 440–447. [CrossRef]
50. Joy, G.; Ananthalakshmi, R.; Vidhya, K. Antibacterial Activity of Biofabricated Molybdenum Nanoparticles. *J. Sci. Ind. Res.* **2021**, *80*, 681–684.
51. Huang, H.L.; Chang, Y.Y.; Chen, H.J.; Chou, Y.K.; Lai, C.H.; Chen, M.Y. Antibacterial properties and cytocompatibility of tantalum oxide coatings with different silver content. *J. Vac. Sci. Technol. A* **2014**, *32*, 02B117. [CrossRef]
52. Seenaa, K.; Bilal, K.; Mohammed, K. Antibacterial activity of NiTi alloy with sputtered tantalum. *J. Univ. Anbar Pure Sci.* **2023**, *17*, 210–224.
53. Yan, S.; Tuozhou, L.; Hongkun, H.; Zixuan, X.; Kai, Z.; Xi, H.; Wenbin, L.; Pengfei, L.; Yihe, H. Differential effect of tantalum nanoparticles versus tantalum micron particles on immune regulation. *Mater. Today Bio* **2022**, *16*, 100340.
54. Kasraei, S.; Sami, L.; Hendi, S.; AliKhani, M.; Rezaei-Soufi, L.; Khamverdi, Z. Antibacterial properties of composite resins incorporating silver and zinc oxide nanoparticles on *Streptococcus mutans* and *Lactobacillus*. *Restor. Dent. Endod.* **2014**, *39*, 109–114. [CrossRef] [PubMed]

55. Siddiqi, K.; Husen, A. Properties of zinc oxide nanoparticles and their activity against microbes. *Nanoscale Res. Lett.* **2018**, *13*, 141. [CrossRef]
56. Mishra, P.; Mishra, H.; Ekielski, A.; Talegaonkar, S.; Vaidya, B. Zinc Oxide Nanoparticles: A Promising Nanomaterial for Biomedical Applications. *Drug Discov. Today.* **2017**, *22*, 1825–1834. [CrossRef]

Disclaimer/Publisher's Note: The statements, opinions and data contained in all publications are solely those of the individual author(s) and contributor(s) and not of MDPI and/or the editor(s). MDPI and/or the editor(s) disclaim responsibility for any injury to people or property resulting from any ideas, methods, instructions or products referred to in the content.